Sub-polar marginal seas fuel the North Pacific through the intermediate water at the termination of the global ocean circulation

Jun Nishioka[a,b]*, Hajime Obata[c], Hiroshi Ogawa[c], Kazuya Ono[a], Youhei Yamashita[d], Keun Jong Lee[c], Shigenobu Takeda[e] and Ichiro Yasuda[c]

[a]Pan-Okhotsk Research Center, Institute of Low Temperature Science, Hokkaido University, Sapporo, Japan
[b]Arctic Research Center, Hokkaido University
[c]Atmosphere and Ocean Research Institute, The University of Tokyo, Kashiwa, Japan
[d]Faculty of Environmental and Earth Science, Hokkaido University, Sapporo, Japan
[e]Graduate School of Fisheries and Environmental Sciences, Nagasaki University, Nagasaki Japan

***Corresponding author**
Jun Nishioka: +81-11-706-7655, nishioka@lowtem.hokudai.ac.jp
ORCID-ID: 0000-0003-1723-9344

Other authors ORCID-IDs
Hajime Obata: 0000-0002-5289-1592,
Hiroshi Ogawa: 0000-0002-4920-8668
Youhei Yamashita: 0000-0002-9415-8743
Shigenobu Takeda: 0000-0002-4997-1583
Ichiro Yasuda: 0000-0002-4742-6880

Classification
Physical Sciences; Earth, Atmospheric, and Planetary Sciences

Keywords: Macro nutrients, Dissolved iron, The North Pacific Ocean, Island chains, Mixing, End of conveyor belt, GEOTRACES

Author Contributions
J.N., H.Ob, and I.Y. contributed to the design of the research. J.N., H.Ob., H.Og. and I.Y. contributed to managing the research cruises. J.N. performed all iron analyses, J.N. and H.Og. performed nutrient analysis, and K.O. was responsible for other onboard

measurements. I.Y. and K.L. measured turbulent mixing parameters in this study. J.N analysed the results and prepared the manuscript with inputs from H.Ob., H.Og., Y.Y. S.T. and I.Y..

This paper includes:

The manuscript, references, methods, figures, and supporting information (figures and tables). We include the 5 main manuscript figures, 8 supporting figures and 2 supporting tables individually.

Abstract

The mechanism by which nutrients in the deep ocean are uplifted to maintain nutrient-rich surface waters in the subarctic Pacific has not been properly described. The iron (Fe) supply processes that control biological production in the nutrient-rich waters are also still under debate. Here, we report the processes that determine the chemical properties of intermediate water and the uplift of Fe and nutrients to the main thermocline, which eventually maintains surface biological productivity. Extremely nutrient-rich water is pooled in intermediate water (26.8–27.6 σ_θ) in the western subarctic area, especially in the Bering Sea basin. Increases of two to four orders in the upward turbulent fluxes of nutrients were observed around the marginal sea island chains, indicating that nutrients are uplifted to the surface and are returned to the subarctic intermediate nutrient pool as sinking particles through the biological production and microbial degradation of organic substances. This nutrient circulation coupled with the dissolved Fe in upper-intermediate water (26.6–27.0 σ_θ) derived from the Okhotsk Sea evidently constructs an area where has one of the largest biological CO_2 drawdown in the world ocean. These results highlight the pivotal roles of the marginal seas and the formation of intermediate water at the end of the ocean conveyor belt.

Significance Statement

A correct understanding of the iron and macro-nutrient dynamics at the termination of the global ocean conveyor belt circulation is critical for understanding the global carbon cycle and its changes in geological time scale. Newly obtained and compiled data sets of iron and macro-nutrients with the vertical mixing magnitude in the subarctic Pacific and marginal seas indicate the processes that determine the nutritional status of intermediate waters and the mechanisms by which sub-polar marginal seas fuel the North Pacific Ocean through the intermediate water. The intermediate water formation processes play a major role in the connection of nutrients between the deep water and the surface water above it, and sustain biological production, at the termination of the global nutrient circulation.

Although the subarctic Pacific is a high nutrient low chlorophyll region (HNLC), where high concentrations of macro-nutrients (hereafter "nutrients") remain in the surface and phytoplankton growth is limited by iron (Fe) availability (1−3), this area has the largest biological CO_2 drawdown among the world oceans (4), and the high productivity of the region's ecosystem and fisheries (5) must be sustained by supplies of both Fe and nutrients into the euphotic zone.

Since the sinking of biogenic particles exports nutrients towards the intermediate/deep sea, the maintenance of surface nutrients requires a return path of the nutrients from the deep ocean (6). In the Southern Ocean, the main nutrient return path from deep water by upwelling and subsequent entrainment into sub-Antarctic mode water has been well explained (6). In the North Pacific high latitude region, nutrients accumulate in deep water with old ^{14}C age (7−9). In previous ^{14}C observations in the North Pacific, the oldest water was clearly observed at approximately 2000−2500 m depth, and the deep water returned southward below the intermediate water (7, 10), which had the highest nitrate and phosphate concentrations, indicating that the high nutrient deep water does not directly affect the surface layer in the subarctic Pacific. Although previous studies imply that the nutrient return path to the surface exists in the northwest corner of the Pacific (6, 11), detailed mechanisms by which nutrients return to the surface layer and how HNLC water is formed in the North Pacific have not been described.

In addition to winter entrainment mixing, an important factor in understanding the return of nutrients to surface water is vertical turbulent diapycnal mixing. Because density stratification in the ocean generally prevents vertical transport (12), it is difficult for dense nutrient-rich deep water and shallow less-dense nutrient-depleted water to be exchanged. Therefore, vertical turbulent mixing is crucial for the quantitative evaluation of the return of nutrients from the deep layer to the surface. An important factor for controlling biological production in the nutrient-rich region is the formation of chemical properties of intermediate water (6), including nutrients and the limiting micro-nutrient “Fe”. North Pacific Intermediate Water (NPIW) is formed under the strong influence of the marginal seas (13−15) and may play a major role in the connection of nutrients between the deep water and the surface water above it (6). Furthermore, additional to atmospheric-dust deposition, recent trace metal measurements have highlighted the importance of localized sources of external Fe, such as river discharge, shelf sediment load, hydrothermal input and sea ice melting (16-21). In the North Pacific, loading Fe from the continental margin and shelves of the marginal seas, from which Fe is transported by intermediate water circulations, are highlighted in recent studies (11, 22-26). There are still debates about the quantitative contributions of atmospheric dust Fe and oceanic Fe transport processes to Fe supply processes in the North Pacific (19, 27−29). To quantitatively elucidate the supply processes of Fe and nutrients to the surface in the North Pacific, it is necessary to comprehensively understand formation of the chemical properties of basin-scale intermediate water, as well as the mixing and circulation in this area (20).

In this study, we compiled comprehensive observed data of chemical water properties (Table S1, which is including newly obtained high quality data from GP02 of GEOTRACES section line, the western Bering Sea, the Aleutian island chains (ICs) and the East Kamchatka Current (EKC)), including dissolved Fe (dFe) and nutrients, with physical parameters of vertical mixing, in the North Pacific including the marginal seas and areas around the Kuril and the Aleutian ICs (Fig. 1a, see Methods). This dataset can be used to analyse the distribution of the chemical parameters of isopycnal surfaces, and we succeed in showing the overall spatial distribution and circulation of Fe and nutrients in the North Pacific for the first time.

Spread of Fe from the Okhotsk Sea via ventilation

We first constructed a diagram showing the 3D distribution of dFe in the North Pacific, including its subpolar marginal seas (the Okhotsk Sea and the Bering Sea) (Fig. 1b). From this dataset, we inferred the characteristics of dFe circulation in the North Pacific. The dFe concentration in surface waters is low throughout the subarctic Pacific region, except for in the shelf areas of the Okhotsk Sea and the Bering Sea (Fig. 1c). The vertical section profile of dFe along GP02 (in Fig. 1b, See SI Appendix, Fig. S1f) was updated to cover the full section from the western to the eastern subarctic Pacific in this study. The eastern side of the subarctic Pacific has a continental shelf source of dFe along the Alaskan Stream (AS) (Fig. 1b, See SI Appendix, Fig. S1f), as previously reported (22). This high-dFe water of the AS is basically confined to the nearshore area, because the boundary current (AS) passes along the coast, although eddy transports of the high-dFe water to offshore occasionally occur (30). The sections also clearly indicate that dFe concentrations are highest in the intermediate water on the western side of the subarctic Pacific (Fig. 1b, See SI Appendix, Fig. S1f) as previous studies suggested (11, 24, 25).

The horizontal distribution indicated by isopycnal analysis in this study clearly shows evidence that the high dFe source in the intermediate waters in the western subarctic Pacific is the marginal seas. The upper (U-) NPIW density range (26.6–27.0 σ_θ, where 26.8 σ_θ is the median density of U-NPIW) is strongly influenced by the Okhotsk Sea Intermediate Water (OSIW), whereas the lower (L-) NPIW density range (27.0–27.5 σ_θ) is influenced mainly by the EKC and the Western Subarctic Gyre (WSG) (13). The isopycnal analysis clearly indicates that the dFe-rich water in the U-NPIW density range (Fig. 1d), in which dissolved oxygen (DO) is also higher than surrounding water (Fig. 2a), is derived from the OSIW that originates in the Okhotsk Sea shelf and propagates along the 26.8 σ_θ isopycnal surface to the western North Pacific (mainly west of 155°E) (Fig. 1d). In contrast, in the L-NPIW density range, e.g., at 27.5 σ_θ (Fig. 1e), dFe is high across a wide area in the western subarctic Pacific, particularly along the northern part of the WSG including the areas southeast of the Kamchatka Peninsula, the western Bering Sea basin and around the eastern Aleutian Islands (hereafter we define the region as "the northern WSG") (Fig. 1e). The dFe distribution in the Oyashio region can be explained by the direct influence of both waters transported from the Okhotsk Sea to U-intermediate water and the EKC influence on L-intermediate water (See SI Appendix, Fig. S2a-f).

Formation of subarctic intermediate water nutrient pool

Intermediate water, which is extremely rich in phosphate (PO_4) but low in DO, was observed on the 26.8 σ_θ isopycnal surface in the northern WSG (Fig. 2a and 2b), especially in the western Bering Sea basin, in the southeast of the Kamchatka Peninsula (Fig. 2a and 2b, See SI Appendix, Fig. S1a and S1b) and around the eastern Aleutian

Islands (Fig. 2a and 2b). In fact, the water was observed in the wide density range of 26.6–27.6 σ_θ (which covers both density ranges of U- and L-intermediate water) along GP02 in the entire subarctic area (See SI Appendix, Fig. S1d and S1e). In addition, the calculated percentage of regenerated (reg-) PO_4 out of the total PO_4 (($AOU \times R_{P:DO}$)/observed $PO_4 \times 100$, see Method) in a section along the EKC line indicates that more than half the total PO_4 in the density range of 26.8–27.6 σ_θ is reg-PO_4 (Fig. 2c). The intermediate water with high proportion of the reg-PO_4 is also observed in the same density range in the subarctic west to east section along the GP02 line (Fig. 2d), indicating that the reg-PO_4-rich intermediate water is widely propagated not only in the northern WSG but also eastward to the Alaskan Gyre (Fig. 2d, See SI Appendix, Fig. S1d and S1e). That is, high nutrients are pooled in the subarctic intermediate water (26.8–27.6 σ_θ, this is greater depth than previous definition of NPIW density range 27.5 σ_θ (13)) in the northern WSG and Alaskan Gyre; we henceforth call the water the "subarctic intermediate nutrient pool (SINP)". Above the SINP, surface productive areas were observed by satellite chlorophyll images in the margin of the northern WSG along the regions of the Oyashio, southeast of the Kamchatka Peninsula, around the Kuril and the Aleutian ICs and the Bering Sea shelf slope (See SI Appendix, Fig. S3). The formation of the chemical properties of the SINP can only be explained by the consumption of DO and regeneration of PO_4, as particulate organic matter that sinks from the surface productive areas decomposes during the intermediate water circulation in the subarctic Pacific and its marginal seas. In contrast, the SINP formation cannot be explained by the direct transport of the nutrient-rich deep water because the deep water has a higher DO concentration.

In the U-NPIW density range, where the influence of Okhotsk Sea water is strong, a meridional vertical cross section of the low percentage of reg-PO_4 along Okh-155 in the Okhotsk Sea to along 155°E in the North Pacific (Fig. 2e) clearly indicates that newly formed (ventilated) water in the Okhotsk Sea which has relatively low PO_4 and high DO (Fig. 2a and 2b) is distributed in the U-NPIW density range, and the U-NPIW circulation mainly transports the preformed (pre-) PO_4 onto the SINP.

Main nutrient return path from the intermediate to the surface

Our data set is mostly collected in summer season. In the dataset, the horizontal distribution of nitrate + nitrite (N) concentrations near the surface (Fig. 3a) are variable, with concentration maxima observed around the Kuril and the Aleutian ICs, whereas the N concentrations at depth on the 26.8 σ_θ surface (Fig. 3b) (in the SINP waters) at the northern WSG are uniformly high. The surface water maxima (Fig. 3a) suggest that upwelling occurs around the ICs. Near these ICs, vertical turbulent fluxes of N from intermediate to surface waters, determined by direct measurements of turbulent vertical diffusivity (using average 100-500 m, see Methods), are two to four orders of magnitude greater than those in the open ocean (Fig. 3c, See SI Appendix, Table S2). The fluxes are largest in the Kuril Straits (average daily N flux, ~100 mmol/m^2/day) and second largest in the Aleutian passes (average daily N flux, ~10 mmol/m^2/day), and in both these regions, they are much greater than the fluxes in the subarctic Pacific (average daily N flux, ~1 mmol/m^2/day) (Fig. 3c, See SI Appendix, Table S2). These results indicate that the Kuril and Aleutian ICs are the hot spots that return nutrients from the intermediate water to the surface water through the enhanced turbulent diapycnal mixing caused by interactions of tidal currents with the rough topography

(31-33). Accounting for the IC areas where turbulent mixing occurs, the estimated uplifted annual N fluxes around the Aleutian and the Kuril ICs (10^{11} ~ 10^{13} mol y^{-1}, geometric mean ~10^{12} mol y^{-1} (See SI Appendix, Fig. S8)) can account for less than 10 % of N pooled in the SINP (4.2 ± 0.4 ×10^{14} mol) per year and comparable to the exported N from surface to below the winter mixed layer in the whole northern subarctic Pacific (~ 10^{12} mol y^{-1}) (34−35) (See SI Appendix, Fig. S4), whereas the estimated flux of uplifted N only by the turbulent mixing in the open ocean in the subarctic Pacific (~ 10^{11} mol y^{-1}; the values estimated by data obtained from KNOT, CL2-CL16, See SI Appendix, Fig. S7) is one order of magnitude smaller than the amount of exported N in this region. The geometric mean of total uplifted annual N flux estimated in this study is ~ 10^{12} mol y^{-1} (See SI Appendix, Fig. S8). The value, however, might be underestimated or there is another missing upward flux of N (or exported N might be overestimated) because the uplifted N flux must be greater than the exported N for maintaining high nutrient surface water in the subarctic Pacific. Together with previously reported information (36), approximately < 1% of N in the SINP is annually transported to NPIW. Additionally, considering the nutrient data with dFe data set analysis, the chemical properties of uplifted intermediate waters around the Aleutian ICs have a lower dFe:N ratio than the diatom demand (see next section). These results indicate that this enhanced mixing around the Aleutian ICs, combined with winter surface mixing, plays an important role in the supply of nutrient-rich (but biologically Fe limited) waters from the SINP to the surface and in maintaining HNLC waters in the surface layer of the subarctic Pacific and the western Bering Sea basin (see next section).

There must be another important role of mixing around the ICs. To balance the nutrient budget in the SINP, the interaction between the deep water and the intermediate water is necessary. Nutrients need to be supplied from the deep water to the SINP by the turbulent mixing processes around the ICs (Fig. 4a, 4b) by the amounts that are laterally transported by the NPIW to low latitudes from the SINP (Fig. 4c, See SI Appendix, Fig. S5). Understanding the nutrient transport interactions between the deep water and the intermediate water will be an issue for the future, and it is necessary to measure turbulence in the abyssal zone.

Intermediate water controls biological productivity

The intermediate water chemical properties are crucial for the productivity of the North Pacific. The nutrient circulation in the SINP coupled with the dFe in U-intermediate water derived from the Okhotsk Sea (external Fe input) (Fig. 1b, Fig. 1d, Fig. 4b) leads to a relatively high dFe:N ratio in the intermediate waters. The dFe:N ratios are higher in the Okhotsk Sea and around the Kuril ICs in the subsurface to intermediate density ranges (Fig. 5a, 5b, 5c) than that around the Aleutian ICs and in the Bering Sea basin (Fig. 5f), indicating that the Fe-rich water diapycnally upwells to the surface around the Kuril ICs by strong turbulent mixing (Fig. 5a, 5b, 5c). The water, which has a high dFe:N ratio, spreads downstream along the Oyashio; the ratio remains high west of 155°E along the U-intermediate water pathway (Fig. 5a and 5d), while the ratio decreases rapidly east of 155°E (Fig. 5a and 5e), probably because of mixing with low-Fe water and scavenging during water transport. In the western subarctic and the Oyashio–Kuroshio transition zone, the upper rim of U-NPIW (isopycnal surface 26.6 σ_θ), which also has a relatively high dFe:N ratio (Fig. 5a), is able to influence the surface water because the shallower isopycnal surfaces at 26.6 σ_θ (~120 m) in the western subarctic Pacific outcrop to the surface in wintertime (Fig. 5d and 5g) (15, 37). The area where these waters with the high dFe:N ratio outcrop corresponds to the area where greater nutrient and biological *p*CO_2 drawdown occur (4, 38). Although the Fe supply is not high enough to prevent Fe limitation (11), which causes persistent HNLC in the subarctic Pacific including around the ICs (39) and the western Bering Sea Basin, Fe supplied from the intermediate water stimulates diatom blooms in the western subarctic and the Oyashio-Kuroshio transition zone (40).

Our results clearly indicate that, in the subarctic Pacific, where high nutrients are distributed (41) at the end of global nutrient circulation (7), sub-polar marginal seas and intermediate waters play pivotal roles for linking deep water to surface biogeochemistry and leading an area with among the highest nutrient concentration in the surface water (41) and the largest biological *p*CO_2 drawdown area in the world ocean (4). We showed the processes determining the chemical properties of intermediate waters (including NPIW), and the mechanisms that determine how intermediate waters affect the supply of Fe and nutrients to the main thermocline and maintain surface productivity. The chemical properties of NPIW likely have a strong influence on biological productivity not only at high latitudes but also at low latitudes in subtropical area due to nutrient and Fe entrainment in the North Pacific (6). The sub-polar marginal seas are changing under the influence of climate change, with changes such as the weakening of ventilation and intermediate water circulation with decreasing sea ice formation (42). Therefore, our findings have important implications for predicting the impact of climate change on the global nutricline, biological productivity and the carbon cycle.

Methods

Field observations.

Comprehensive observations for investigating Fe in the North Pacific were carried out from 1998 to 2018. Vertical profiles of dissolved Fe concentrations were collected in 24 cruises, which included marginal seas. All cruises that observed the dFe data are listed in Table S1. Seawater from the surface to bottom layers was collected with acid-cleaned Teflon-coated 10 or 12 L Niskin-X bottles that were mounted on a CTD (SBE 9 plus) with a carousel multi-sampling system (SBE32) during all cruises in this study. The details of the sampling methods used for each cruise have been described elsewhere (11, 24, 25, 26, 40, 44, 45).

Dissolved Fe measurements

To sub-sample from the Niskin-X sampler during the R/V *Hakuho Maru* cruise, the samplers were transported in a clean air bubble (filled with air that had been passed through a high-efficiency particulate air filter). To sub-sample from the Niskin-X sampler during the R/V *Professor Multanovskiy, Professor Kromov* cruise, the samplers were placed in a clean tent. A 0.22 μm Millipak filter (Millipore co.) or a 0.2 μm Acropak filter (Pall Co.) was connected to the Niskin-X spigot; then, the filtrate was collected in acid-cleaned 125-mL low density polyethylene (LDPE) bottles (Nalgene Co., Ltd). We confirmed that there were no significant differences between the dFe concentrations measured using the Acropak filter and the Millipak filter (See SI Appendix, Fig. S6b).

Before 2006, the filtrate (<0.22 μm and 0.2 μm) was directly adjusted to pH 3.2 with a formic acid (10 M)–ammonium (2.4 M) buffer. After 2006, the filtrate (<0.22 μm and 0.2 μm) was adjusted to pH < 2 by the addition of ultrapure HCl (Tamapure AA-10) and then allowed to remain at least for 24 h to three months at room temperature in the onboard clean room. Each sample was then adjusted to pH 3.2 just before measurements by the addition of an ammonium solution and a formic acid (10 M)–ammonium (2.4 M) buffer. Then, dFe, defined as the leachable Fe in the filtrate at pH < 2, was analysed in the onboard or onshore laboratory using a flow-injection analysis (FIA) chemiluminescence detection system (46). All sample treatments were performed under laminar flow in the onboard or onshore clean-air laboratory. We confirmed that there were no significant differences between these two different acidified methods for open ocean sample (See SI Appendix, Fig. S6a).

The quality of dFe measurements was controlled by measuring house standard seawater. Additionally, the dFe measurements and reference seawater analyses in this study after 2006 were quality-controlled using SAFe (Sampling and Analysis of Iron) cruise (47) reference standard seawater (obtained from the University of California Santa Cruz for an inter-comparison study). We measured a SAFe reference sample during every sample measurement run of the FIA instrument performed in the onboard and onshore laboratories in the cruise for the GEOTRACES program (Table S1). The consensus values for Fe(III) in the SAFe reference standard seawater are 0.093 ± 0.008 nM (S) and 0.933 ± 0.023 nM (D2) (May 2013, www.geotraces.org), and, in GEOTRACES official cruise, for instance, we obtained values of 0.098 ± 0.010 nM (n = 12) (S) and 0.976 ± 0.101 nM (n = 10) (D2) using our method. This good agreement demonstrates that our data quality was high and that our data are comparable with the global GEOTRACES dataset. The detection limit (three times the standard deviation of the Fe(III) concentration (0.036 nM) of purified seawater that had been passed through an 8-quinolinol resin column three times to remove Fe) was 0.020 nM. See ref. (11, 24, 25, 26, 40, 44, 45).

Nutrient measurements

Nutrient (nitrate + nitrite, phosphate, silicate) concentrations were also analyzed in water samples collected from the same stations. Nitrate + nitrite (define as N in this study) concentrations were measured using a BRAN-LUEBBE auto-analyser (TRACCS 800), and a BL-Tec auto-analyser (QuAAtro). Most of the nutrient measurements in this study were quality-controlled using KANSO reference material (KANSO Co.). In this study, we also refer nutrient data from JAMSTEC MR04-04 cruise (http://www.godac.jamstec.go.jp/darwin/cruise/mirai/mr04-04/j)

Other parameters

Salinity and temperature were measured using a conductivity-temperature-depth (CTD) sensor, and dissolved oxygen (DO) concentrations were measured using an oxygen sensor connected to a CTD. The DO concentration was also measured on board by the Winkler titration method, and the DO concentration obtained by the sensor was calibrated using the concentration determined by the Winkler method. The oxygen solubility was calculated and apparent oxygen utilization (AOU) was then calculated as the difference between the solubility and the measured DO concentration.

Calculation for percentage of regenerated (reg-) PO_4

The percentage of regenerated (reg-) PO_4 in total PO_4 was calculated by the equation "(AOU×$R_{P:DO}$)/observed PO_4×100". In this equation, $R_{P:DO}$ is a regenerated mol ratio for phosphate to oxygen; we employed a $R_{P:DO}$ of 170 from reference (48).

Estimating vertical fluxes of dFe and nitrate

The material flux was estimated at the Kuil and the Aleutian ICs. We employed a simple calculation to estimate the vertical flux of dFe and N from the subsurface to the surface at the ICs using the following equations.

$$\text{dFe Flux} = K_\rho \times(\text{dFe/dz}), \quad \text{N Flux} = K_\rho \times(\text{dN/dz})$$

Our measured dFe and N vertical profiles at the ICs strait were already influenced by the strong mixing, and the gradients (dFe/dz and dN/dz) in the profiles from surface to subsurface were disrupted. Thus, the gradients in the profiles at the IC strait were not suitable for estimating the material flux from intermediate water to surface water. To evaluate the flux from the intermediate water to the surface water at the IC straits, we used the vertical profile of dFe and N obtained around the straits (locations are blue dots in See SI Appendix, Fig. S7), which we used to approximate the profiles before the water was influenced by the mixing process. The surface to subsurface gradients of dFe (dFe/dz) and N (dN/dz) were evaluated at all stations located around the straits (blue dots for the ICs and yellow dots for the subarctic Pacific). To estimate fluxes, we combined the gradients with the measured snapshot of vertical diffusivity $K\rho$ (=$0.2\varepsilon N^{-2}$ where ε is turbulent kinetic energy dissipation rate in W/kg and $N^2 = -g\rho_z/\rho$ where N^2 is squared buoyancy frequency, where g and ρ are the gravitational acceleration and reference potential density, respectively) for depths of 100-500 m. The $K\rho$ was measured by using a free-fall vertical microstructure profiler (VMP2000 Rockland Scientific International co.) (31, 32, 33) on the cruise Kh06, Kh07, KH-09-4 for the ICs waters and on the cruise KH-08-2 for the open waters in the western subarctic Pacific (See Table S2). The $K\rho$ was also measured by using CTD-attached fast-response thermistors (AFPO7, Rockland Scientific International co.) (49, 50) on the KH-17-3 cruise for open water in the subarctic Pacific (See Table S2). Comparison study between these two measurement methods have been conducted at 100 stations in several cruises (50), including KH-09-4 (See Table S2) (50). Turbulence intensity estimated from CTD-fast-response thermistors was compared to those by free-fall microstructure profilers, conducted at the same location within 2h, and the result was reported in Goto et al. (2018) (50) where ε is valid for $10^{-10} < \varepsilon < 10^{-8}$ W/kg after response correction (49) and data screening (50), and it has been confirmed that ε from both measurement methods are comparable and within a factor of 3 (50).

Estimated budget of nitrate+nitrite (N) among the surface, intermediate, and deep waters (See SI Appendix, Fig. S4, Fig. S8)**.**

The annual transport of N from the SINP to the surface was calculated by the geometric mean of uplifted N fluxes at the Kuril and Aleutian ICs accounting for the approximate area where mixing occurs (the Kuril ICs: 1.12469E+11 m^2 and Aleutian ICs: 2.14087E+11 m^2, the IC areas were defined to cover where the depth-integrated tidal energy dissipation rate estimated from a global barotropic tide model (51) were higher than 5.0×10^{-2} W/m^2 along the ICs) (See SI Appendix, Fig. S8). The uplifted N flux in the open ocean in the subarctic Pacific was calculated by the geometric mean fluxes in the subarctic Pacific, accounting for the area of the northern WSG (4.92255E+12 m^2) and Alaskan Gyre (3.02873E+12 m^2). Exported N from the surface through the winter mixed layer depth was calculated by using number of 1.49~2.3 mol-C m^{-2} y^{-1}, which was previously reported in the WSG (34, 35) and the Alaskan Gyre (35), accounting for the area of the northern WSG and Alaskan Gyre (See SI Appendix, Fig. S8). N pooled in the SINP was calculated with an average N concentrations (42 ± 2.3 μmol/kg) in the intermediate water range between 26.8-27.6 at the stations, the thickness of the intermediate water (1237 ± 137 m), in the whole subarctic Pacific and the western Bering sea, and the area of the northern WSG and Alaskan Gyre (See SI Appendix, Fig. S8).

Ocean Data View parameters.

Ocean Data View (ODV; http://odv.awi.de/) (52) was used to calculate and produce plots for the basin-scale isopycnal surface distribution and vertical section profiles of each parameter in Figs. 1, 2, 3, 5, Fig. S1, S2, S5, S7.

Data availability.

The data that support the findings of this study are available at the site of following URL. https://eprints.lib.hokudai.ac.jp/*******

Acknowledgements

We would like to thank the captain, crew and scientists on board the all research vessels listed in Table S1 for their help with observations and sample collection. Thanks to Dr. Y. N. Volkov and Mr. Scherbinin, the Far Eastern Regional Hydrometeorological

Research Institute, for their cooperation with the Japanese-Russian joint research program. Thanks to Dr. Wakatsuchi, Ms Aiko Murayama and Dr. Toru Hirawake for their helpful support for this study. Thanks to Dr. Hiroaki Saito and Dr. Yu Umezawa for their nutrient measurement for the samples obtained during cruise KH-15-4. This work was supported by the Grant-in-Aid for Scientific Research, the Ocean mixing processes: OMIX project, (Grant Numbers JP15H05820, JP15H05817, 17H00775) funded to JN, HOb, IY, the Arctic Challenge for Sustainability (ArCS) project, and the Grant for Joint Research Program of the Institute of Low Temperature Science, Hokkaido University.

References

1. J. H. Martin, S. E. Fitzwater, Iron deficiency limits phytoplankton growth in the north-east pacific subarctic. *Nature* **331,** 341-343 (1988).
2. A. Tsuda et al., A mesoscale iron enrichment in the western subarctic Pacific induces large centric diatom bloom. *Science* **300,** 958-961 (2003).
3. P. W. Boyd *et al.*, The decline and fate of an iron-induced subarctic phytoplankton bloom. *Nature* **428,** 549-553 (2004).
4. T. Takahashi *et al.*, Global sea–air CO2 flux based on climatological surface ocean *p*CO2, and seasonal biological and temperature effects. *Deep Sea Research part II* **49,** 9–10, 1601-1622 (2002).
5. Y. Sakurai, An overview of Oyashio ecosystem. *Deep Sea Res. Part II* **54,** 2526-2542 (2008)
6. J. L. Sarmiento, N. Gruber, M. A. Brzezinski, J. P. Dunne, High-latitude controls of thermocline nutrients and low latitude biological productivity. *Nature* **427,** 56-60 (2004).
7. W. S. Broecker, T.-H. Peng, *Tracers in the sea*, (Lamont-Doherty Geological Observatory, Columbia University, 690 pp doi:10.2307/1309641 1982).
8. K. Matsumoto, R. M. Key, Natural radiocarbon distribution in the deep Ocean. *Global Environmental Change in the Ocean and on Land*, Eds., M. Shiyomi et al., pp. 45-58. Terapub (2004).
9. K. Matsumoto, Radiocarbon-based circulation age of the world oceans. *J. Geophys. Res.* **112: C09004,** doi: 10.1029/2007JC004095 (2007).
10. M. Kawabe, S. Fujio, Pacific Ocean ciroculation based on observation. *J. Oceanogr.* **66,** 389-403 (2010).

11. J. Nishioka *et al.*, Intensive mixing along an island chain controls oceanic biogeochemical cycles. *Global Biogeochem. Cycle* **27,** 920–929 (2013).
12. J. L. Sarmiento, N. Gruber, *Ocean Biogeochemical dynamics* (Princeton University press, Princeton, New Jersey 2006).
13. I. Yasuda, The origin of the North Pacific Intermediate Water. *J. Geophys. Res.* **102(C1),** 893-909 (1997).
14. I. Yasuda *et al.*, Hydrographic structure and transport of the Oyashio south of Hokkaido and the formation of North pacific Intermediate Water. *J. Geophys. Res.* **106(C4),** 6931-6942 (2001).
15. L. D. Talley, An Okhotsk Sea Water anomaly: Implications for ventilation in the North Pacific. *Deep Sea Res., Part I* **38,** S17 (1991).
16. P. W. Boyd, M. J. Ellwood, The biogeochemical cycle of iron in the ocean. *Nature Geo.* **3,** 675-682 (2010).
17. T. M. Conway, J. G. Seth, Quantification of dissolved iron sources to the North Atlantic Ocean. *Nature* **511,** 212–215 (2014).
18. A. Tagliabue *et al.,* Surface-water iron supplies in the Southern Ocean sustained by deep winter mixing. *Nature Geo.* **7,** 314-320 (2014).
19. A. Taliabue, O. Aumont, L. Bopp, The impact of different external sources of iron in the global carbon cycle. *Geophys. Res. Lett.* **41,** 920-926 doi:10.1002/2013GL059059, (2014).
20. A. Tagliabue *et al.*, The integral role of iron in ocean biogeochemistry. *Nature* **543,** 51-59 (2017).
21. J. A. Resing *et al.*, Basin-scale transport of hydrothermal dissolved metals across the South Pacific Ocean. *Nature* **523,** 200-203, doi:10.1038/nature14577 (2015).
22. P. J. Lam *et al.*, Wintertime phytoplankton bloom in the subarctic Pacific supported by continental margin iron. *Global Biogeochem. Cycle* **20,** GB1006, doi:10.1029/2005GB002557 (2006).
23. P. J. Lam, J. K. B. Bishop, The continental margin is a key source of iron to the HNLC North Pacific Ocean. *Geophys. Res. Lett.* **35,** L07608, doi.org/10.1029/2008GL033294 (2008).
24. J. Nishioka *et al.*, Iron supply to the western subarctic Pacific: Importance of iron export from the Sea of Okhotsk. *J. Geophys. Res.* **112,** C10012 https://doi.org/10.1029/2006JC004055 (2007).
25. J. Nishioka, H. Obata, Dissolved iron distribution in the western and central subarctic Pacific: HNLC water formation and biogeochemical processes. *Limnol. Oceanogr.* **62 (5),** 2004-2022 (2017).

26. J. Nishioka *et al.*, Quantitative evaluation of iron transport processes in the Sea of Okhotsk. *Prog. Oceanogr.* **126**, 180-193 (2014).
27. M. Schulz *et al.*, Atmospheric transport and deposition of mineral dust to the ocean: implication for research need, *Environ. Sci. Technol.* **46**, (19), 10390–10404, doi: 10.1021/es300073u (2012)
28. A. Ito, Z. Shi, Delivery of anthropogenic bioavailable iron from mineral dust and combustion aerosols to the ocean, *Atmos. Chem. Phys.* **16,** 85-99, doi.org/10.5194/acp-16-85-2016, (2016).
29. E. R. Sholkoviz, P. N. Sedwick, T. M. Church, A. R. Baker, C. F. Powell, Fractional solubility of aerosol iron: Synthesis of a global-scale data set. *Geochem. Cosmochim. Acta* **89**, 173-189, doi.org/10.1016/j.gca.2012.04.022 (2012).
30. W. K. Johnson, L. A. Millar, N. E. Sutherland, C. S. Wong, Iron transport by mesoscale Haida eddies in the Gulf of Alaska, *Deep-Sea Res. II* **52,** 933-953 (2005).
31. S. Itoh *et al.*, Strong vertical mixing in the Urup Strait. *Geophys. Res. Lett.* **38,** L16607, doi:10.1029/2011GL048507 (2011).
32. S. Itoh, I. Yasuda, T. Nakatsuka, J. Nishioka, Y. N. Volkov, Fine-and microstructure observation in the Urup Strait, Kuril Islands, during August 2006. *J. Geophys. Res.* **115,** C08004, doi:10.1029/2002JC005629 (2010).
33. M. Yagi, I. Yasuda, Deep intense vertical mixing in the Bussol' Strait. *Geophys. Res. Lett* **39,** L01602, doi:10.1029/2011GL050349 (2012).
34. H. I. Palevsky, P. D. Quay, D. E. Lockwood, D. P. Nicholson, The annual cycle of gross primary production, net community production, and export efficiency across the North Pacific Ocean. *Global Biogeochem. Cycle,* 361-380, doi:10.1002/2015GB005318 (2016).
35. M. Wakita et al., Biological organic carbon export estimated from the annual carbon budget observed in the surface waters of the western subarctic and subtropical North Pacific Ocean from 2004 to 2013. *J. Oceanogr.* 72, 665- 685, 10.1007/s10872-016-0379-8 (2016).
36. Y. Long, X-H. Zhou, X. Guo, The Oyashio Nutrient Stream and its Nutrient Transport to the Mixed Water Region. *Geophys. Res. Lett.* **46,** 1513–1520, doi.org/10.1029/2018GL081497 (2019).
37. T. Suga, M. Motoki, Y. Aoki, A. M. MacDonald, The North Pacific climatology of winter mixed layer and mode waters. *J. Phys. Oceanogr.* **34,** 3-22 (2004).
38. S. Yasunaka, *et al.*, Mapping of sea surface nutrients in the North Pacific: Basin-wide distribution and seasonal to interannual variability. *J. Geophys. Res.* **119,** 11 doi.org/10.1002/2014JC010318, (2014).

39. K. Suzuki *et al.*, Spatial variability in iron nutritional status of large diatoms in the Sea of Okhotsk with special reference to the Amur River discharge, *Biogeosciences* **11,** 2503–2517 doi: 10.5194/bg-11-2503-2014, (2014).
40. J. Nishioka, T. Ono, H. Saito, K. Sakaoka, T. Yoshimura, Oceanic iron supply mechanisms which support the spring diatom bloom in the Oyashio region, western subarctic Pacific. *J. Geophys. Res.* **112,** C10012, doi: 10.1029/2010JC006321 (2011).
41. World Ocean Atlas, National Centers for environmental information, NOAA, https://www.nodc.noaa.gov/OC5/woa18/ 2018
42. K. I. Ohshima, S. Nihashi, K. Iwamoto, Global view of sea-ice production in polynyas and its linkage to dense/bottom water formation. *Geosci. Lett.* **3,** doi:10.1186/s40562-016-0045-4 (2016).
43. A. Marchetti, M. Maldonado, E. S. Lane, P. J. Harrison, Iron requirements of the pennate diatom Pseudo-nitzschia: Comparison of oceanic (High-nitrate, low-chlorophyll waters) and coastal species. *Limnol. Oceanogr.* **51,** 2092-2101, doi:10.4319/10.2006.51.5.2092 (2006).
44. J. Nishioka, S. Takeda, C. S., W. K. Wong, Johnson Size-fractionated iron concentrations in the northeast Pacific Ocean: distribution of soluble and small colloidal iron. *Mar. Chem.* **74,** 157-179, doi.org/10.1016/S0304-4203(01)00013-5 (2001).
45. J. Nishioka et al., Size-fractionated iron distributions and iron-limitation processes in the subarctic NW Pacific, *Geophys. Res. Lett.* **30(14),** doi:10.1029/2002GL016853 (2003).
46. H. Obata, H. Karatani, E. Nakayama, Automated determination of iron in seawater by chelating resin concentration and chemiluminescence detection. *Anal. Chem.* **65**, 1524–1528 (1993).
47. K. S. Johnson et al., Developing standards for dissolved iron in seawater. *EOS* **88**, 131–132 (2007).
48. L. A. Anderson, J. L. Sarmiento, Redfield ratios of remineralization determined by nutrient data analysis. *Global Biogeochem. Cycles* **8,** 65-80 (1994).
49. Y. Goto, I. Yasuda, M. Nagasawa, Turbulence estimation using fast-response thermistors attached to a free-fall vertical microstructure profiler. *J. Atmos. Ocean Tech.* **33,** 2065-2078. doi: 10.1175/JTECH-D-15-0220.1 (2016).
50. Y. Goto, I. Yasuda, M. Nagasawa, Comparison of turbulence intensity from CTD-attached and free-fall microstructure profilers. *J. Atmos Ocean Tech.* **35,** 147-162. doi: 10.1175/JTECH-D-17-0069.1 (2018).

51. Y. Tanaka, I. Yasuda, H. Hasumi, H. Tatebe, and S. Osafune, 2012: Effects of the 18.6-year modulation of tidal mixing on the North Pacific bidecadal climate variability in a coupled climate model, Journal of Climate, 25, 7625-7642 (2012).
52. R. Schlitzer, *Ocean Data View*. http://odv.awi.de (2018).

Figure legends

Figure 1

Comprehensive observation for investigating dissolved Fe in the North Pacific conducted from 1998 to 2018. a) Observed stations for dataset and water current in the subarctic Pacific, b) 3D dissolved Fe diagram in the North Pacific constructed by the dataset (part of data is not included), GP02 in b) is line ID for the GEOTRACES program, c) horizontal distribution of dissolved Fe at surface (5-10m), d) same as c) but at isopycnal surface 26.8 σ_Θ, e) same as c) but at isopycnal surface 27.5 σ_Θ.

Figure 2

a) Horizontal distribution of dissolved oxygen at isopycnal surface 26.8 σ_Θ, b) same as a) but phosphate, c) vertical section profile of proportion of regenerated phosphate along Line East Kamuchatka Current (EKC) in b), d) same as c) but along GP02 line in b), e) same as c) but along Okh-155 in b), (※ Nutrient include the data referred from JAMSTEC, MR04-04 cruise data, http://www.godac.jamstec.go.jp/darwin/cruise/mirai/mr04-04/j). Black solid line in c, d, e indicate isopycnal surface of 26.8, 27.0, 27.5 σ_Θ, respectively.

Figure 3

a) horizontal distribution of nitrate+nitrite (N) concentration at surface (5-10m), b) same as a) but isopycnal surface 26.8 σ_Θ, Note that the color scale is different between Fig.3a and Fig.3b. c) Vertical upward fluxes of N around the Kuril Islands chain, Aleutian Islands chain, and the subarctic Pacific. d) Same as c) but for dissolved Fe. (※ Nutrient for a) and b) include the data referred from JAMSTEC, MR04-04 cruise data, http://www.godac.jamstec.go.jp/darwin/cruise/mirai/mr04-04/j)

Figure 4

The schematic draw of the circulation and intermediate water formation processes of nutrients and dissolved Fe in the North Pacific, a) through the Bering Sea, b) through the Okhotsk Sea, c) horizontal circulation. Regenerated nutrients and dissolved Fe in the intermediate water are vertically supplied to surface layer by turbulent mixing around the ICs and cycle between the intermediate and the surface layer. This nutrient circulation in the intermediate water is coupled with intermediate dFe discharge from the Okhotsk Sea. Then, nutrient and Fe are transported to eastward and to low latitude by the NPIW, which influence to biological production at some hot spot in the North Pacific.

Figure 5

a) Horizontal distributions of dissolved Fe to N ratio (nM/μM) at isopicnal surface 26.6 σ_Θ in the North Pacific. b) Dissolved Fe vs nitrate+nitrite (N) plots, with Fe and N demand ratio by dominated diatom (Black solid line used 3 μmol Fe/mol C (ref 43) for calculate Fe vs N), in Okhotsk sea shelf and the East Sakhalin, c) Same as b) but data around the Kuril strait, d) Same as b) but data from 155˚E to the west. e) Same as b) but data from 155˚E to the East, f) Same as b) but data around the Aleutian straits and in the Bering Sea Basin. Color in b-f indicate water density (σ_Θ). In the area b, c, d, the Upper-intermediate water has high dissolved Fe concentration relative to N at a level to relax & release iron limitation. In the area e and f, the Upper-intermediate water contain not sufficient Fe for diatom growth. g) horizontal distributions of depth at isopicnal surface 26.6 σ_Θ, which depth is outcropped by winter mixing processes in the western subarctic and the Oyashio-Kuroshio transition zone.

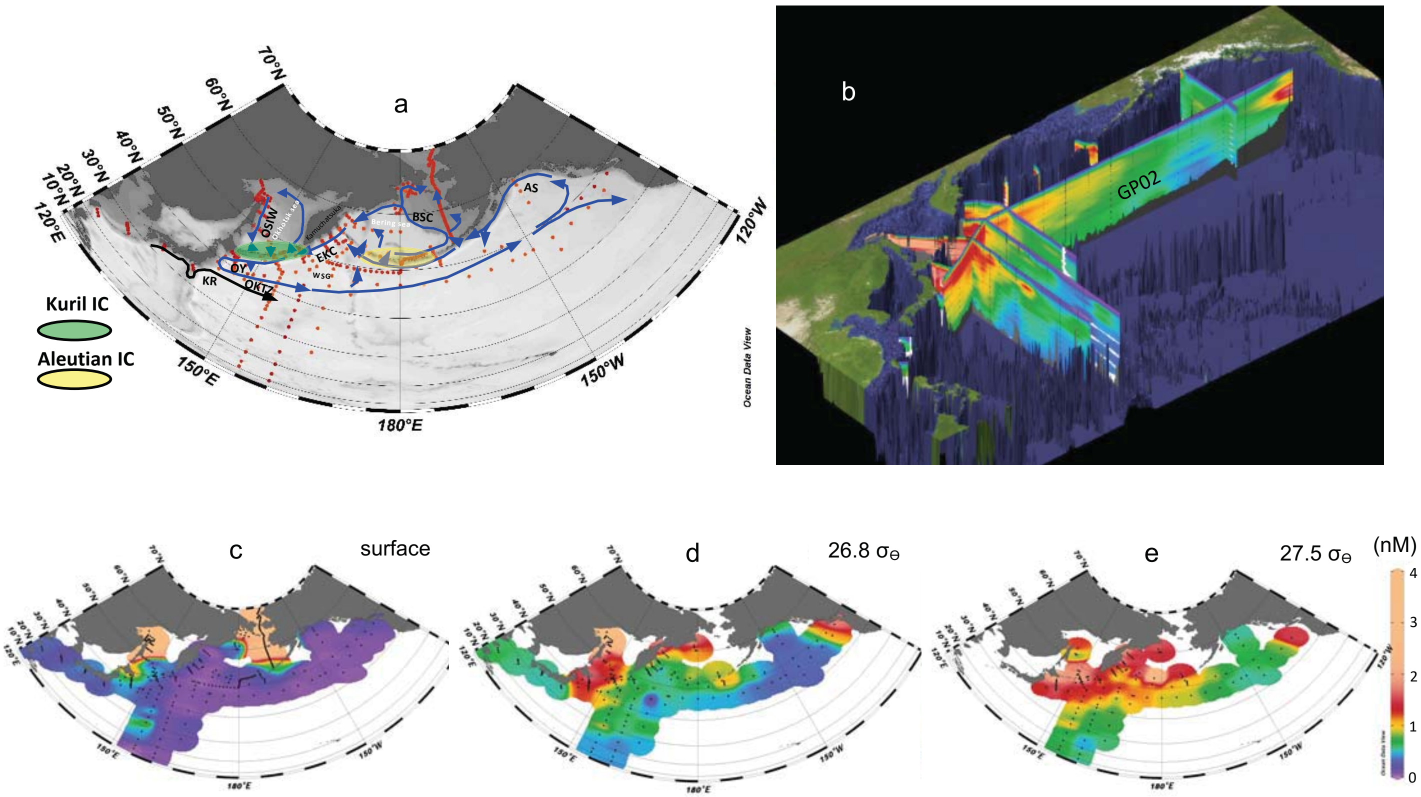
a
70°N
60°N
50°N
40°N
30°N
20°N
10°N
120°E
OSIW
BSC
AS
EKC
OY
KR
OKTZ
WSG
Kuril IC
Aleutian IC
150°E
180°E
150°W
120°W
Ocean Data View
b
GP02
c
surface
d
26.8 σθ
e
27.5 σθ
(nM)
4
3
2
1
0

Figure 1

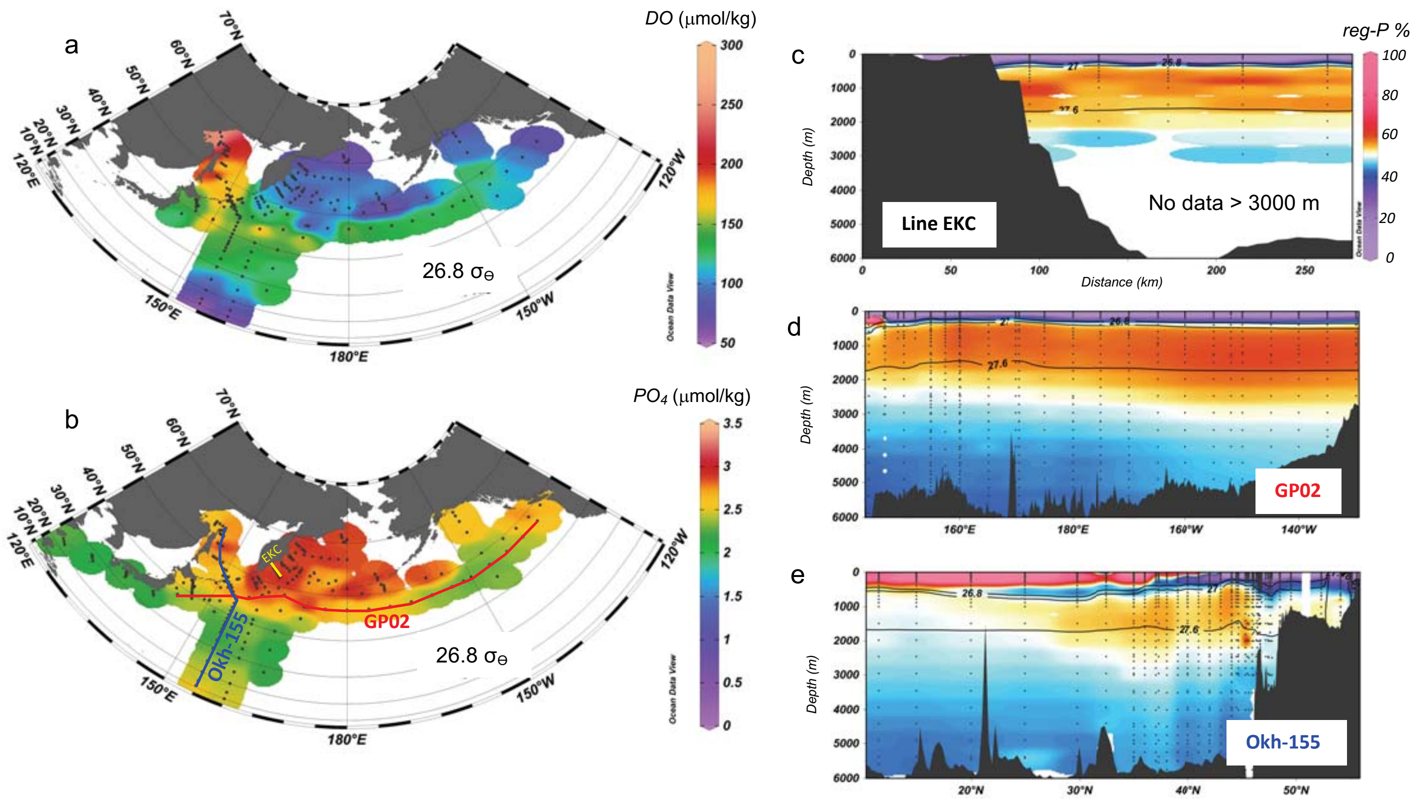

a
b
c
d
e
DO (μmol/kg)
PO4 (μmol/kg)
reg-P %
26.8 σΘ
Line EKC
No data > 3000 m
GP02
Okh-155
EKC
Depth (m)
Distance (km)

Figure 2

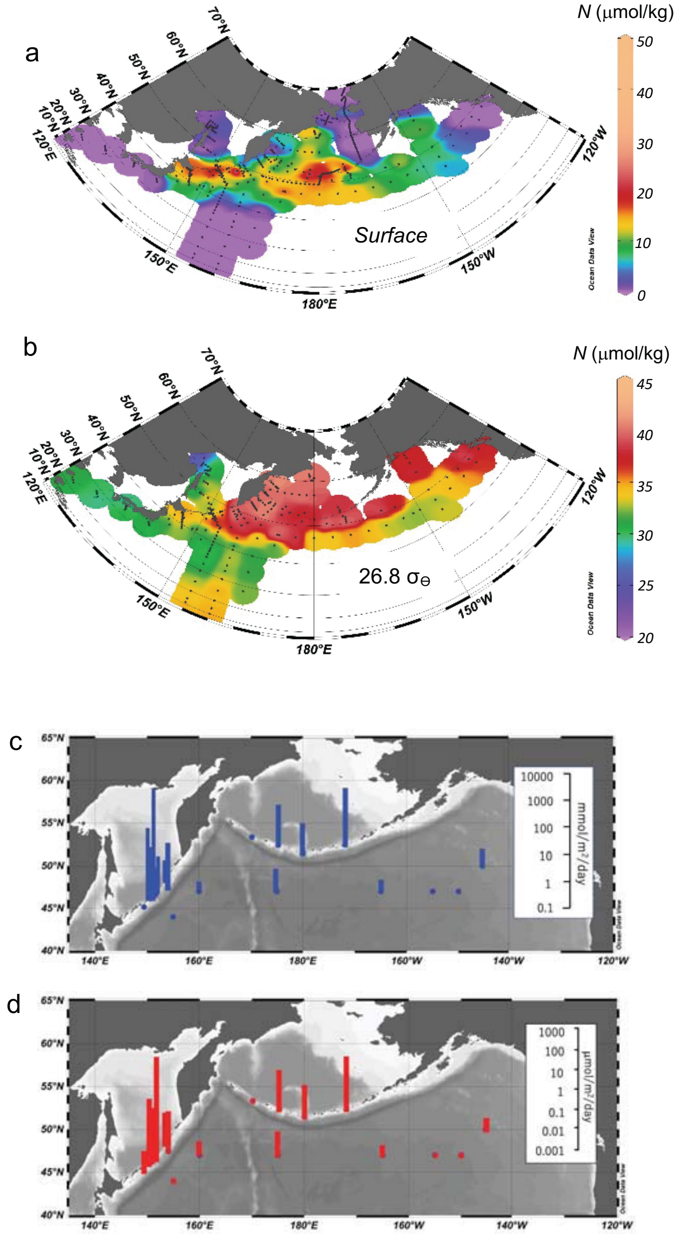
a
N (μmol/kg)
Surface
b
N (μmol/kg)
26.8 σΘ
c
mmol/m²/day
d
μmol/m²/day
Ocean Data View

Figure 3

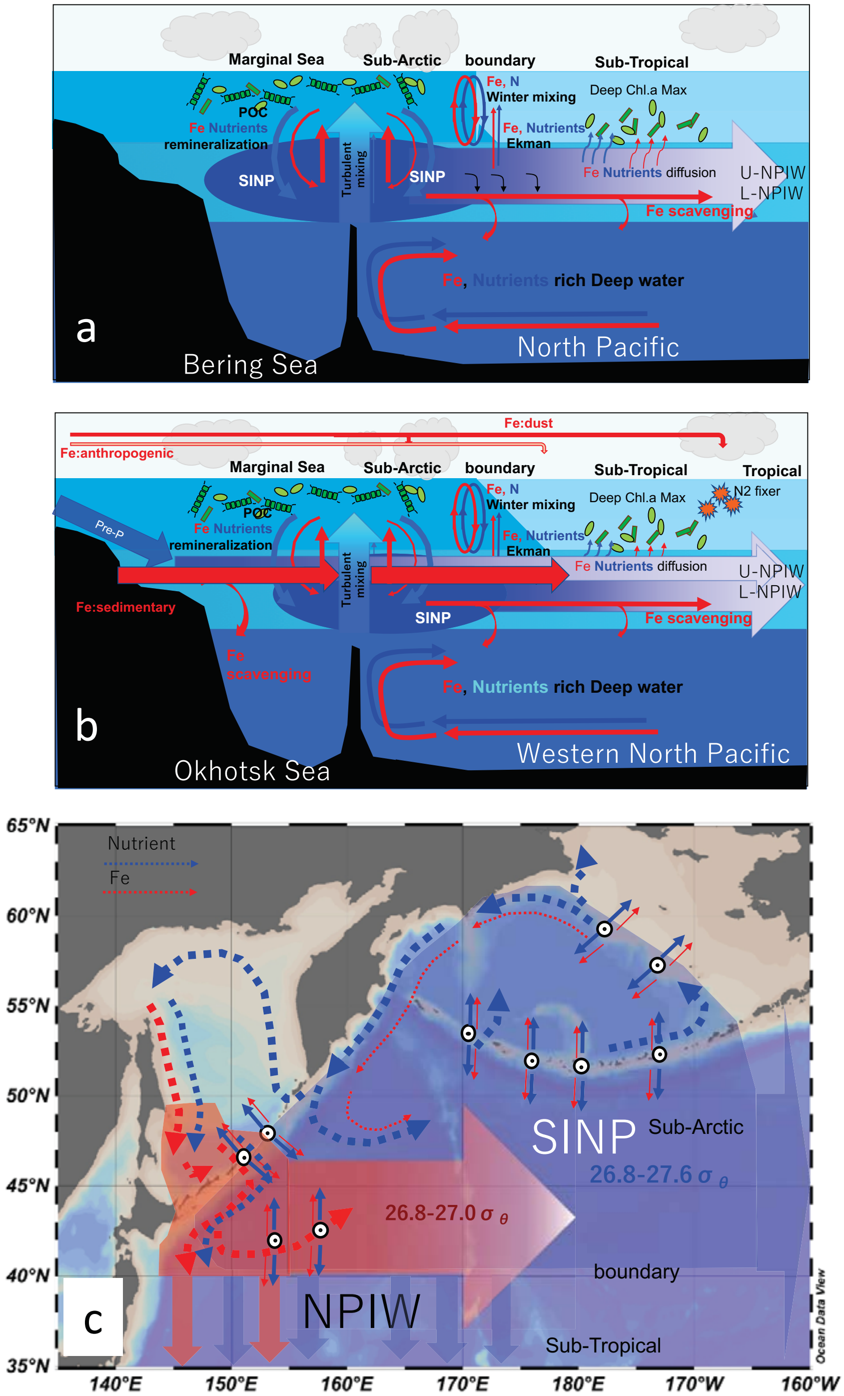
Marginal Sea
Sub-Arctic
boundary
Sub-Tropical
POC
Fe Nutrients
remineralization
Fe, N
Winter mixing
Fe, Nutrients
Ekman
Deep Chl.a Max
Fe Nutrients diffusion
SINP
Turbulent mixing
U-NPIW
L-NPIW
Fe scavenging
Fe, Nutrients rich Deep water
a
Bering Sea
North Pacific
Fe:dust
Fe:anthropogenic
Tropical
N2 fixer
Pre-P
Fe:sedimentary
Fe scavenging
b
Okhotsk Sea
Western North Pacific
Nutrient
Fe
SINP
Sub-Arctic
26.8-27.6 σ θ
26.8-27.0 σ θ
boundary
NPIW
Sub-Tropical
c
65°N
60°N
55°N
50°N
45°N
40°N
35°N
140°E
150°E
160°E
170°E
180°E
170°W
160°W
Ocean Data View

Figure 4

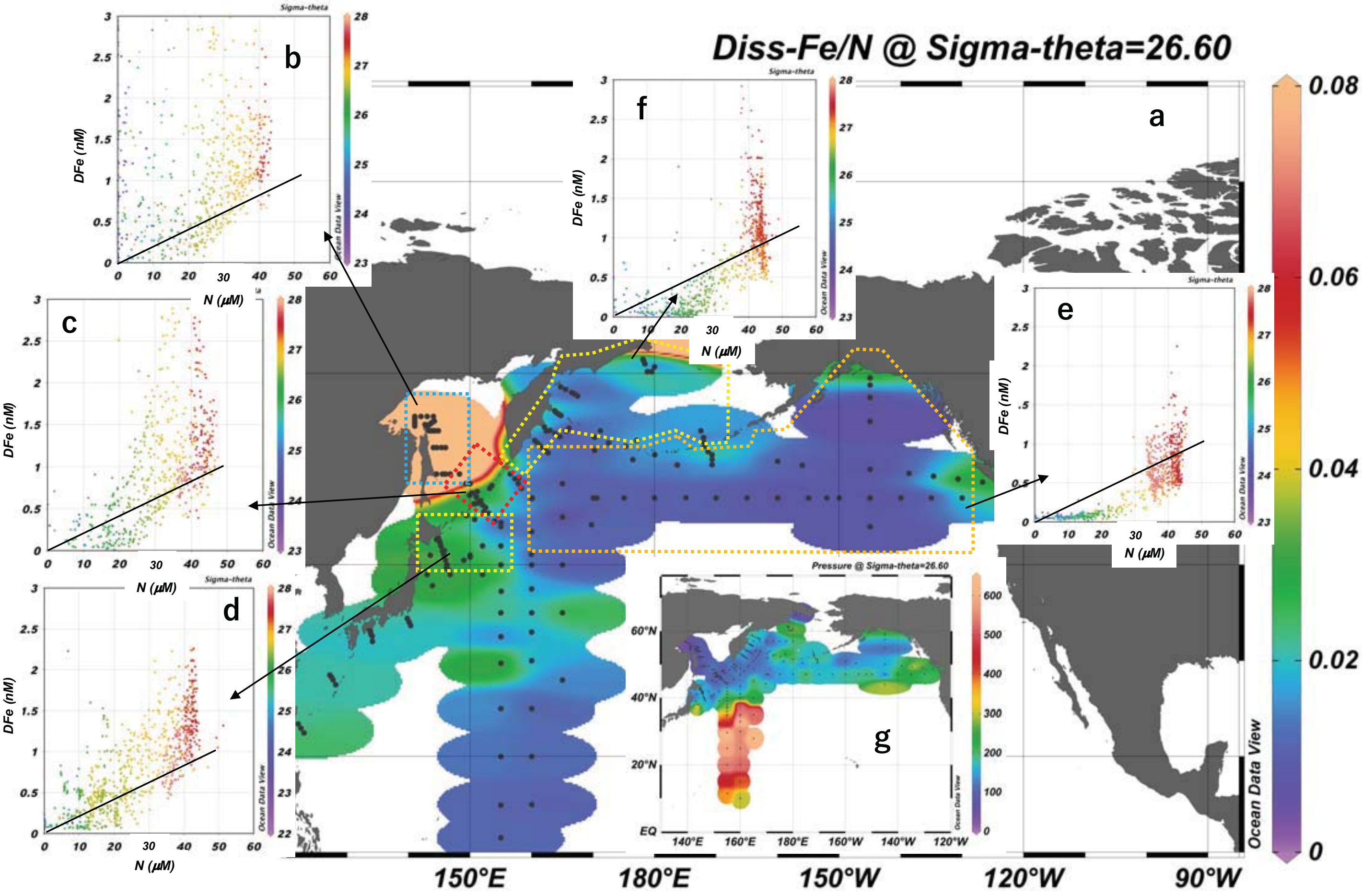

Diss-Fe/N @ Sigma-theta=26.60
a
b
c
d
e
f
g
DFe (nM)
N (μM)
Sigma-theta
Ocean Data View
Pressure @ Sigma-theta=26.60
150°E
180°E
150°W
120°W
90°W
0.08
0.06
0.04
0.02
0

Figure 5